A Combined Numerical and Experimental Investigation of Transition in a Laminar Separation Bubble

M. Lang, O. Marxen, U. Rist, S. Wagner

Universität Stuttgart, Institut für Aerodynamik und Gasdynamik (IAG), Pfaffenwaldring 21, 70550 Stuttgart, Germany

lang@iag.uni-stuttgart.de

Summary

A laminar boundary layer separates in a region of adverse pressure gradient, undergoes transition, and finally the turbulent boundary layer reattaches, forming a laminar separation bubble (LSB). Laminar-turbulent transition within such a LSB is investigated by means of Laser-Doppler-Anemometry (LDA), Particle Image Velocimetry (mono PIV and stereoscopic PIV (SPIV)) and direct numerical simulation (DNS).

A method is presented to measure the amplification of small unsteady disturbances by means of phase-locked PIV. The role of unsteady disturbances with and without controlled spanwise variation in the occurring mechanism of transition are examined in detail. Observations for the development of small disturbances are compared to predictions from linear stability theory.

1 Introduction

Laminar-turbulent transition plays an important role in aerospace aerodynamics because of its influence on drag. When a laminar boundary layer separates due to an adverse streamwise pressure gradient, the flow is subject to increased instability with respect to small-amplitude disturbances. Laminar-turbulent transition will occur and in the considered case of a LSB the turbulent boundary layer will reattach. The occurrence of boundary-layer separation essentially affects the efficiency of the whole system, e.g. the wing of a sailplane or even a commercial aircraft. In the latter case the Reynolds number for a deployed slat lies in the same range as for a wing of a sailplane. Beside its influence on drag, the occurrence of a LSB causes noise. This an important aspect in consideration of wind-turbine blades.

Despite several fundamental investigations on transition in a laminar separation bubble (e.g. [1, 2, 3]), it is still difficult to predict and understand processes leading to breakdown of the separated shear layer. Though reliability of results from 3-D DNS is now commonly accepted, no detailed comparison of numerical results with

experimental data obtained in a LSB has been made up to now, in particular for unsteady phenomena. In the present work it will be shown that by mutual comparison of results from modern measurement techniques and 3-D DNS, mechanisms leading into breakdown to turbulence in existing experimental facilities can be identified in a way that is not possible when applying only one of these methods. Due to the sensitivity of the transition process, non-intrusive measurement techniques such as LDA and PIV are suitable and reliable instruments for quantitative flow characterization.

The experiments were carried out in a laminar water tunnel which was especially designed to study transition in Blasius boundary layers and in separation bubbles [4]. Wiegand [5] investigated boundary layer transition initiated by a point source using hot-film anemometry. Thereby, he also confirmed the high quality of the tunnel flow with a turbulence level of less than 0.05%. The low turbulence level in the free stream allows investigations on amplification of intentionally excited disturbances and their influence on transition. Because of large temporal and spatial scales in water, this facility is also particularly suitable for flow visualization.

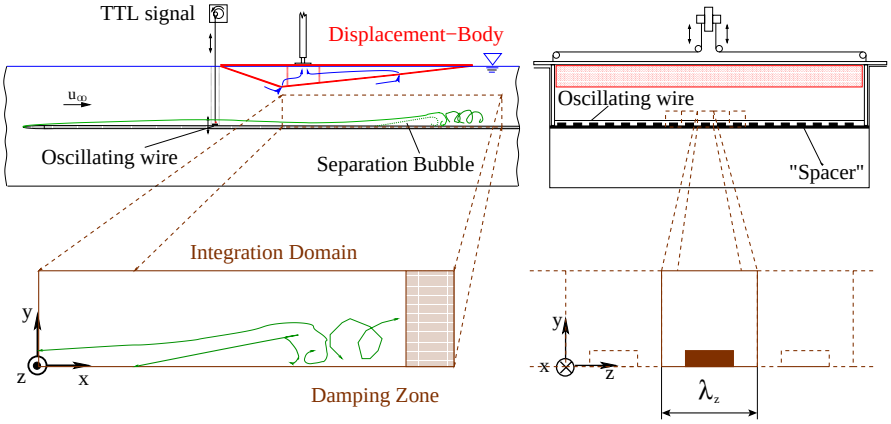

Figure 1 Experimental set-up in the laminar water-tunnel and numerical integration domain

2 Experimental and Numerical Methods

2.1 Experimental Set-Up

A flat plate with an elliptical nose is mounted in the test section of the laminar water tunnel. At the end of the flat plate, a screen leads to a pressure difference between the upper and the lower side. Therefore, fluid transport is forced through a gap between the flat plate and the tunnel side-walls. This prevents the formation of an unstable corner boundary-layer, therefore extending the range of laminar flow on the plate. At a free stream velocity of $u_\infty = 125\ \frac{mm}{s}$ a shape factor of $H_{12} = 2.6$

was measured. Over a spanwise range of $-200\,mm < z < 200\,mm$ it varies only about $\pm 1\%$. Therefore, the boundary layer can be approximately assumed to be a two dimensional Blasius boundary-layer.

To generate a pressure-induced laminar separation bubble, a displacement body is positioned in the test section above the plate (Fig. 1). After a short region of favorable pressure gradient, the adverse pressure gradient is applied. This is a common technique and was also used in [2]. In following statements and diagrams the origin of the used coordinate system is in the narrowest section under the displacement body on the center line of the flat plate.

In the laminar water tunnel, a displacement body with a simple triangular shape is used. The cross section ratio of $1 : 1.43$ and the opening angle of 5.1° after the narrowest section under the displacement body were first chosen according to streamwise applied pressure distributions from available DNS data. Finally, these parameters were adjusted by flow visualization. The separation bubble had to have a certain size to allow high resolution measurements, but it had not to become too large because of long measurement times in water with the LDA. The boundary layer developing on the displacement body is sucked off in the narrowest section and through another suction strip in the region of adverse pressure gradient. This prevents separation and transition on the displacement body itself. The necessary suction rate was ascertained by flow visualization.

The experiment is performed under controlled conditions to suppress low frequency background disturbances (flapping, [6]) which occur under natural (undisturbed) conditions. Therefore a small amplitude 2-D Tollmien-Schlichting wave (TS-wave) is forced by an oscillating wire. The wire is positioned in the critical layer in the region of favorable pressure gradient ($x = -230\ mm$). The power unit of the disturbance source generates a TTL trigger signal each period which is taken as time reference for phase-locked measurements. To stay close to the natural case the disturbance amplitude was very weak compared to other investigations (e.g. [7]). The fundamental frequency $f_0 = 1.1\ Hz$ was chosen to match the most amplified frequency according to linear stability theory. In the undisturbed (natural) case, vortex shedding occurs with the same frequency, but with varying amplitudes (flapping) when compared to the case with disturbance input. Further investigations on the influence of different initial disturbance levels are already given in [8] so that the amplitude in the present case was fixed.

To generate a 3-D disturbance, thin ($1.2\ mm$) metal plates are placed regularly underneath the wire. These so-called "spacers" cause a steady 3-D disturbance mode which interacts with the TS-wave. This results in a three-dimensional wave combination with typical peak-valley structure, where the boundary layer thickens stronger in the peak plane compared to the valley plane (Fig.2) [9, 10]. An advantage of 3-D disturbance input is that vortex structures, appearing with the onset of transition, are fixed in spanwise direction. In the present measurements with 3-D disturbance input, the spanwise wavelength was set to $\lambda_z = 58\ mm$, so that regularly appearing spanwise vortex structures could be seen in the transition region (Fig. 3). Flow visualization using the hydrogen bubble technique was carried out to determine the spanwise wavelength. Fig. 3 shows a simultaneous view of the xy-

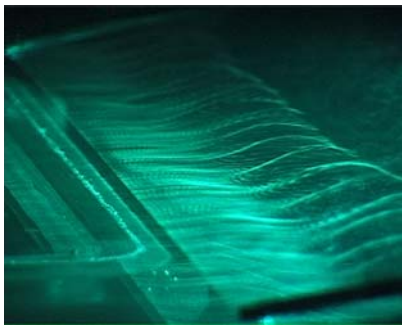

Figure 2 3-D disturbance-wave combination

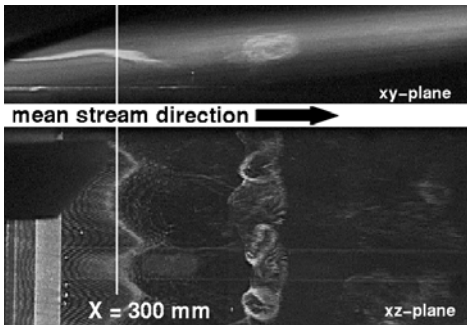

Figure 3 Vortex structures in the transition region visualized by the hydrogen bubble method.

and xz-plane. For this image, a mirror was positioned beneath the flat plate.

The applied 2-component LDA measures the velocity components $u(t)$ in mean flow direction and $v(t)$ perpendicular to the flat plate. In order to achieve near-wall measurements with the probe aligned almost perpendicular to the side walls (to avoid astigmatism), the lower beam can be shifted towards the optical axis of the probe. However, this halves the beam intersection angle for the vertical velocity component v, thus causing a higher noise level compared to the streamwise component u. The lowest turbulence level measurable with the LDA is 0.8% for the u velocity [9]. In contrast to hot-film anemometry, LDA is a non-intrusive measurement technique which provides the possibility to identify velocities with their value and direction. In the transition region of the shear layer with its strong bidirectional velocity fluctuations, this is an important benefit. Thus, the dividing streamline can be determined directly from the measured velocity profiles.

The PIV system was built up in corporation with the "Deutsches Zentrum für Luft- und Raumfahrt" (DLR) and was expanded to a stereoscopic system (SPIV). It consists of a double pulsed Nd:YAG-laser (Quantel Twins, $2 \times 150mJ$), two high resolution CCD-cameras (PCO Sensicam, $1280\,px \times 1024\,px$) and an external sequencer (DLR).

The good optical access to the test section allows PIV and SPIV measurements in all cartesian planes. To minimize optical distortions (e.g. astigmatism) due to diffraction in water, the optical axis of the camera has to be aligned almost perpendicular to the border of the two optical media. Therefore, in case of SPIV measurements, water filled prisms or tanks with mirrors were mounted at the tunnel sidewalls to allow different viewing angles of $\pm 45^\circ$ to the measurement volume.

2.2 Numerical Method and Calculation Parameters

Spatial direct numerical simulation (DNS) of incompressible flow is used to compute the pressure induced LSB described in the previous section. In the numerical

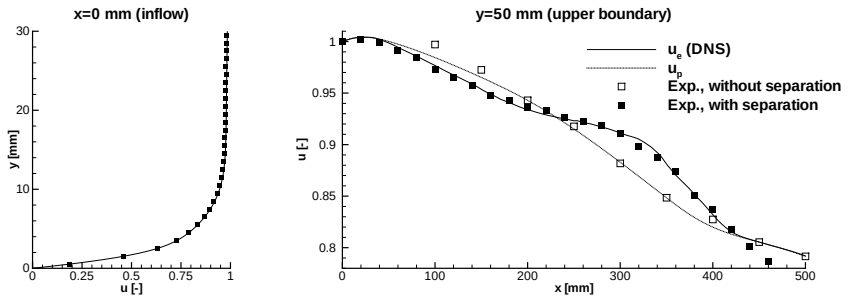

Figure 4 Streamwise mean velocity at $x = 0\ mm$ (left) and $y = 50\ mm$ (right). DNS results u_e (solid line), potential velocity u_p prescribed in DNS (dotted line); Measurements with (filled symbols) and without separation (open symbols).

method, fourth-order accurate finite differences are used for downstream and wall-normal discretization, while a spectral ansatz is applied in spanwise direction. A fourth-order Runge-Kutta scheme is used for time integration. Upstream of the outflow boundary a buffer domain smoothly returns the flow to a steady laminar state. The streamwise pressure gradient is imposed by prescribing a potential velocity distribution for the streamwise velocity u_p at a constant distance y from the wall, while the displacement effect of the boundary layer is captured by a boundary-layer interaction model. The numerical method applied in this study is described in detail in [11]. A small-amplitude 2-D Tollmien-Schlichting (TS) wave is forced upstream of the LSB. Additional 3-D disturbances are excited to trigger the break-up of the separated shear layer into regions of small-scale turbulence.

Parameters of the flow are chosen to match the experimental set-up introduced before. The length of the computational box in streamwise direction is $x \approx 800\ mm$, with the inflow placed at the position of the narrowest section (Fig. 1). The height of the box is $y = 50\ mm$ in wall-normal direction, corresponding to approximately 12.5 times the displacement thickness δ_1 of the incoming boundary layer. In spanwise direction a single spacer wavelength fits into the domain ($z = \lambda_z = 58\ mm$). The resolution is 185 and 1778 grid points in wall-normal and streamwise direction, respectively. One TS wave is discretized with approximately 120 grid points. In spanwise direction, 27 Fourier modes are computed. The resolution was confirmed to be sufficient by a calculation with increased number of grid points (approximately by a factor of 1.5 in each direction) yielding the same results in the first part of the LSB, which are discussed in this paper.

The velocity profile at the inflow boundary was obtained from a preceeding 2-D DNS of a strongly accelerated boundary layer (starting from a Blasius solution well upstream of the displacement body in the experiment) with the favorable pressure gradient chosen to match the experimental values up to the narrowest section [12], since the measured profile could not be represented by an analytical (Falkner-Skan) solution ($H_{12} \approx 1.6$ at the inflow). As can be seen in Fig. 4, the u-velocity profile from measurements and computations at $\hat{x} = 0\ mm$ are in excellent agreement.

Hence, this profile is expected to be an appropriate inflow condition for the subsequent DNS of the LSB.

The potential velocity distribution u_p is chosen according to measurements where separation was suppressed by artificially causing transition prior to the laminar separation point (Fig. 4). It serves as initial condition at the free-stream boundary in the DNS and finally the mean edge velocity distribution u_e almost matches the experimental measurements with separation bubble. Since this velocity condition at the upper boundary is not fixed, but rather comes out of the boundary-layer interaction model, it can already be considered a result of the DNS. Good agreement of DNS data with experiments (Fig. 4) therefore gives a first proof of the comparability of the separation bubbles observed in the experiment and in the DNS. Furthermore, it should be emphasized that the actual velocity prescribed at the upper boundary is unsteady and the results presented in the diagram are time-averaged.

2.3 Data Acquisition and Analysis

In order to obtain temporal and spanwise wavenumbers in case of 3-D disturbance input, velocity profiles were measured in spanwise direction over one spacer wavelength. A double Fourier transform of in time and span yields the amplitudes $a_{h,k}$ and phases $\Phi_{h,k}$ of this disturbance [10].

$$\begin{aligned} u'(x,y,z,t) &= \sum_{h=1}^{H} a_h(x,y,z)\sin(h2\pi f_0 t + \phi_h(x,y,z)) \\ &= \sum_{h=1}^{H}\sum_{k=-K}^{K} a_{h,k}(x,y)\sin(h2\pi f_0 t - k\frac{2\pi}{\lambda_z}z + \phi_{h,k}(x,y)), \end{aligned}$$

The indices h and k denote the wave-number coefficients in time and spanwise direction and specify the (h,k)-modes of this double Fourier transform. This method can be used until small-scale and strong non-periodic 3-D structures occur downstream saturation in the reattachment region of the laminar separation bubble.

LDA measurements were performed starting from the beginning of adverse pressure gradient until shortly beyond the onset of disturbance saturation. The resolution of the flow field in streamwise direction was $\Delta x = 10\,mm$ in the transition region. In case of 3-D disturbance input the spanwise wave length was sampled with 16 boundary-layer profiles. A step size of $\Delta y = 1\,mm$ in wall normal direction provided a resolution of boundary-layer profiles with about 25-30 points depending on the local boundary-layer thickness. Record length of all measured points was about 30 wire cycles. To evaluate the entire spectrum of the measured data, time-signals were cut to multiples of the wire cycle. For an exact determination of amplitudes and phases of the fundamental frequency and its higher harmonics a phase-averaging technique with respect to the disturbance source was used [9, 13]. Due to long measurement times with LDA in water, small structures cannot be sufficiently resolved.

Here a PIV (SPIV) system with its high spatial resolution provides better results concerning the detection of structures in the transition region.

In case of amplitude measurements by PIV the field of view was about $58 \times 50\,mm^2$. With a sampling window size of $32\,px \times 32\,px$ and a step-size of $16\,px$ the resolution of wall-normal boundary-layer profiles was up to $40-50$ points and consequently higher than obtained by LDA measurements. To capture TS-amplitudes phase-locked measurements with respect to the disturbance source were carried out. The phase angle was shifted over 18 time-steps to sample one TS-period. For each phase angle 30 measurements were averaged. A Fourier analysis of 18 instantaneous boundary layer profiles then yields the TS-amplitude with its higher harmonics.

The recorded data-sets have been dewarped (in case of SPIV) and evaluated with a FFT based cross-correlation method. A Levenberg-Marquardt peak-fitting algorithm provides sub-pixel accuracy and minimizes the peak-locking effects [14]. Unreasonable vectors (in general less than 2%-5%) were deleted and re-interpolated by a fit to their neighbors.

In DNS, data from four TS cycles are Fourier analyzed in time using a Hanning window function to suppress the influence of low frequency drifting of the bubble. This drift would otherwise contaminate the Fourier-analyzed signals. The low level of subharmonic disturbances resulting from this way of data processing confirms the clear distinction of drifting and TS frequency, supporting the validity of this procedure.

3 Results

In the present results the Reynolds number based on the displacement thickness at the separation line is about $Re_{\delta_1} = 900$. The extent of the laminar separation bubble of about $250\ mm$ is given by the mean dividing streamline with the net mass flux set to zero [3, 15] (Fig. 5).

$$\int_{y=0}^{y_d} \bar{u}(y)dy = 0$$

Since the LSB is of highly unsteady character, it appears inevitable to consider time- and space-resolved disturbance quantities before claiming that the same physics are captured in the numerical and experimental investigations. This shall be done in the following paragraphs for 2-D and 3-D disturbance input. The first section of the LSB is dominated by a primary convective instability of the 2-D TS-wave (see [16]). Therefore, the development of 2-D time harmonics (TS-wave) appears to be very important and is examined in detail.

Note that for the input of a 2-D disturbance only the oscillating wire is used (generating a TS-wave). In case of 3-D disturbance input the oscillating wire is used in combination with spacers as emphasized before. These cause steady 3-D disturbances which, together with the TS-wave (2-D time harmonic), generate additional unsteady 3-D disturbance modes (oblique waves). Thus, the case of 2-D disturbance input is also included in the case of 3-D disturbance input.

3.1 2-D disturbance input (TS-wave)

A detailed comparison of boundary layer quantities from LDA measurements, LST and DNS under consideration of a 2-D disturbance is given in [15, 13]. A very good agreement was obtained for unsteady quantities as well as for the base flow variables. Now, additional PIV measurements were performed in the region of linear amplification (LST) until beyond onset of disturbance saturation. The obtained mean quantities and amplitude distributions shall be compared to LST and LDA results in this section.

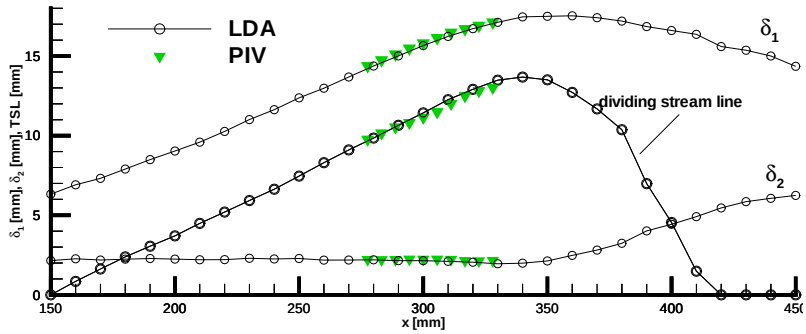

Figure 5 Comparison of boundary-layer mean quantities obtained from LDA and PIV measurements with 2-D disturbance input (TS-wave)

To capture the TS-amplitudes, 30 phase-locked measurements with respect to the disturbance source were carried out. Thereby, the phase angle was shifted over 18 time steps to sample one TS-period. The absolute mean value computed from the whole datasets yields mean flow variables. Fig. 5 shows a very good agreement of displacement thickness, momentum loss thickness and the dividing streamline in the saturation region, obtained from PIV data in comparison with LDA measurements.

Furthermore, it can be shown, that by phase-locked measurements, the accuracy of PIV is sufficient not only to measure instantaneous data. It is also a suitable instrument to measure small-amplitude ($< 5\%$) unsteady phenomena. A Fourier analysis of 18 averaged instantaneous boundary-layer profiles yields wall-normal amplitude distributions of the fundamental frequency (TS-wave) and its higher harmonics. For validation, a comparison with results of LST and corresponding LDA-measurements are given in Fig. 6(a-d).

Solving the Orr-Sommerfeld equation for the mean velocity profiles obtained from PIV data, amplitude distributions according to LST are computed. These results of LST are based on measured mean velocity profiles which must be determined very accurately because their second derivative plays an important role in the Orr-Sommerfeld equation.

Fig. 6(a,b) shows very good agreement of PIV measured wall-normal amplitude distributions $(1,0)$ with predictions of LST normalized by their maximum value.

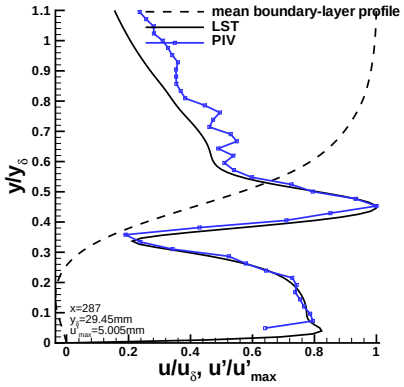

(a) PIV measured amplitude distribution $u'(\frac{y}{y_\delta})$ of the (1,0)-mode in comparison with linear stability theory for streamwise position $x = 287\,mm$

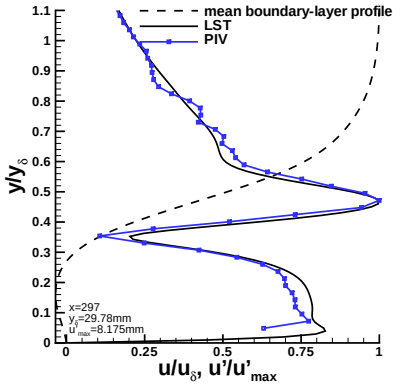

(b) PIV measured amplitude distribution $u'(\frac{y}{y_\delta})$ of the (1,0)-mode in comparison with linear stability theory for streamwise position $x = 297\,mm$

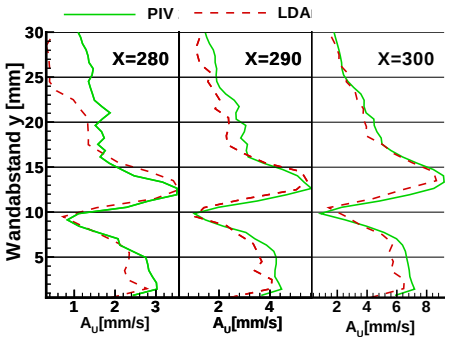

(c) PIV measured amplitude distributions $u'(y)$ of the (1,0)-mode in comparison with appropriate LDA measurements for three streamwise positions

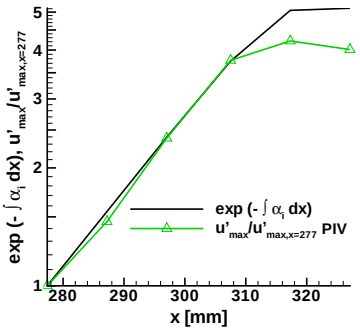

(d) Amplification $u'_{max}(x)$ of the (1,0)-mode measured by PIV in comparison with amplification according to linear stability theory

Figure 6 Comparison of measured unsteady phenomena by PIV with predictions of linear stability theory and LDA measurements

Additionally, comparisons with LDA measurements are given in Fig. 6(c) for three streamwise positions, which were carried out for reference (not normalized). As can be seen by the very good agreement with LST and LDA data in Fig. 6(a,b,c), the PIV evaluation provides reasonable accuracy even in the region with strong velocity gradient for the component u (shear-layer maximum).

Streamwise amplification of u'_{max} (shear-layer maximum) obtained by PIV is

drawn in Fig. 6(d) normalized by $u'_{x=277\,mm}$. The amplification curve of this disturbance mode matches predictions of LST very well until the onset of saturation downstream $x = 310\,mm$. Here, a rapid 3-D development takes place leading to breakdown of the separated shear layer.

The possibility of measuring unsteady phenomena by means of PIV has one important benefit: The time to perform the previously described verification measurements, to prove the quality of the experimental set-up, could be decreased by more than a factor of 10 in comparison to adequate LDA measurements.

3.2 3-D disturbance input

Results from LDA measurements and DNS

General properties of the LSB are first discussed using base-flow variables. Here, base flow means averaged quantities in time and spanwise direction. Note that the LSB is a highly unsteady phenomenon, and the base flow can never be observed instantaneously at any time step.

In Fig. 7 a comparison of some boundary-layer quantities is shown. The boundary-layer displacement thickness δ_1 considerably increases along the separation bubble, while the momentum-loss thickness δ_2 starts to grow not until the onset of transition. Good agreement between DNS results and measurements reveals that a separation bubble of approximately the same size is formed in both cases.

As can be seen in Fig. 7 the boundary-layer parameters over the separated region are nearly the same for a 2-D or 3-D disturbance input, as can be seen also from investigations of Augustin et al. [17]. This confirms that the development of the 2-D TS wave is decisive for the transition process in the considered case and the

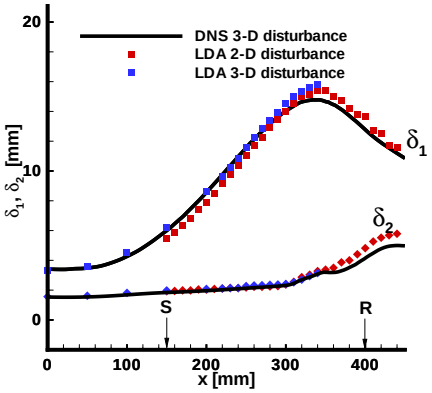

Figure 7 Boundary-layer mean quantities from beginning of adverse pressure gradient ($x = 0\,mm$) until beyond reattachment.

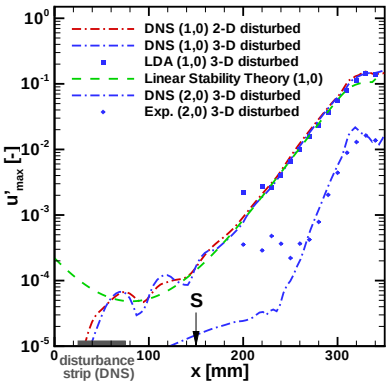

Figure 8 Amplification of the maximum velocity fluctuation u'_{max}. Results from DNS (lines), measurements (symbols) and LST.

disturbed steady 3-D mode (caused by spacers) only plays a minor role.

Results for the development of unsteady phenomena will show a comparison of amplitude distributions and streamwise amplification of the supplied 3-D wave combination obtained by LDA measurements and DNS. Using Mono-PIV it is also possible to measure unsteady 3-D disturbance modes as it was shown in the previous section for the 2-D case. Therefore, measurements were performed by scanning one spacer wave-length with the light sheet in z-direction to resolve the spanwise deformation of the separated shear layer. The results are discussed in [18].

Fig. 8 shows the amplification curve for streamwise velocity fluctuations u'. Mode $(1,0)$ (TS-wave) is strongly amplified in the region of separated shear layer. Experimental and numerical results perfectly match from $x = 230\ mm$ onwards even shortly beyond saturation. Good agreement with linear stability theory (LST) confirms the primary convective nature of the disturbance. Amplitude development predicted by LST is obtained by integrating amplification rates in streamwise direction. As can be seen from Fig. 8, calculation and experiment also predict the same amplitude, growth rate and saturation level for the non-linearly generated higher harmonic disturbance $(2,0)$. Both disturbances saturate at the position of shear-layer roll-up.

Wall-normal distributions of amplitudes and phases of both measured velocity components are compared to LST and DNS in Fig. 9 at a location around the middle of the region of linear amplification. The detached shear-layer corresponds to the part of maximum gradient for the u velocity around $y = 13\ mm$. It is at this distance from the wall where the disturbance amplitude of the 2-D TS wave (1,0) reaches

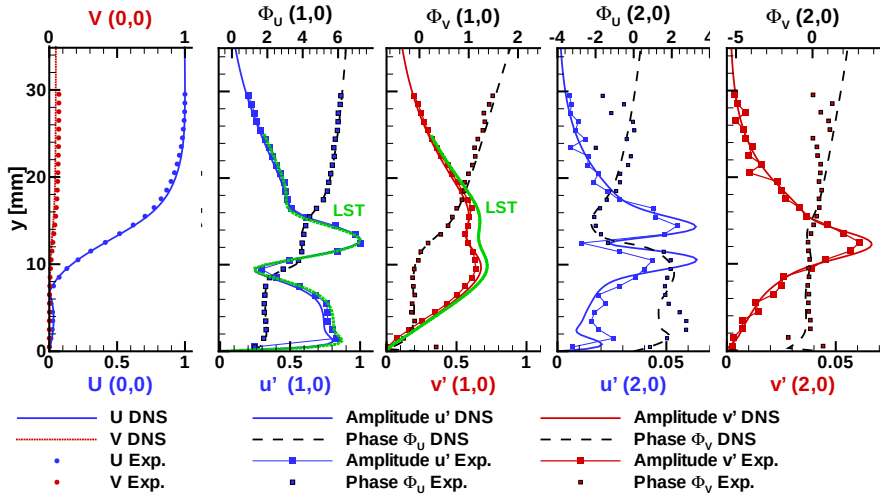

Figure 9 Comparison of measured wall-normal amplitude distributions (LDA) with linear stability theory and DNS for the (1,0)-mode (TS-wave) and its first higher harmonic with 3-D disturbance input

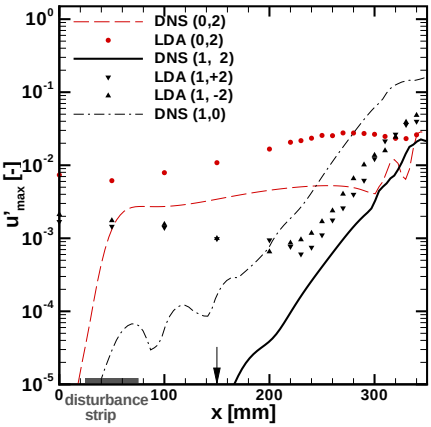

Figure 10 Amplification of the maximum velocity fluctuation u'_{max}. Results from DNS (lines) and measurements (symbols).

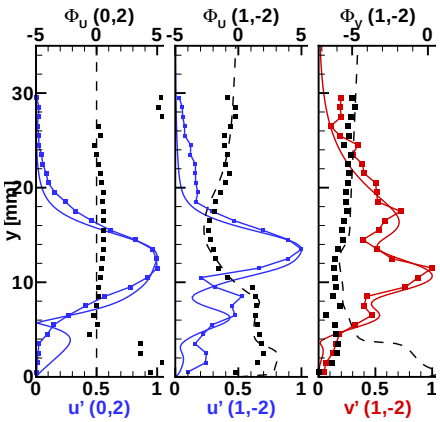

Figure 11 Normalized 3-D amplitude and phase distributions. Results from DNS (lines) and measurements (symbols) at $x = 290\ mm$.

maximum values for the u-velocity, as in the case of a Kelvin-Helmholtz instability. The measured amplitudes of these 2-D time harmonics perfectly match DNS results even for the first higher harmonic (2,0). All amplitude distributions shown in Fig. 9 are normalized in respect to the maximum amplitude $u'_{max}(1,0)$ of the TS-wave.

In the experiment, a strong initial steady disturbance $(0,2)$ with half the spacer wavelength can be observed (Fig. 10). Differences to the DNS are due to a long transient development, depending on the way the disturbance is introduced. A detailled investigation on the behaviour of this steady disturbance is given in [19]. For the considered case it is important that the unsteady modes $(1, \pm 2)$ show the same amplification to explain the transition mechanism. From good agreement with LST for the development of the 2-D TS wave, as described in the previous section, it can be concluded that the spanwise modulation of the base flow does not exert any influence on 2-D instability characteristics of the flow field. In contrast, the growth of spanwise modulated perturbations of fundamental frequency $(1, \pm 2)$ is decisively affected by the presence of this steady mode. The growth rate of these disturbances cannot be explained by linear theory, nor by a secondary (convective [8] or temporal [16]) instability, since it already sets in well before the TS wave has gained a sufficiently large amplitude.

Instead, non-linear interaction between the TS wave $(1,0)$ and the large steady disturbance $(0,2)$ generates modes $(1,\pm 2)$ with nearly the same amplification rate as mode $(1,0)$. Results from a spanwise-symmetrical DNS confirm this fact by showing the same growth rate for mode $(1,2)$ only in the presence of a large steady disturbance. Agreement of amplitude and phase distributions between experiment and DNS is reasonable (Fig. 11), albeit some deviations from symmetry can be seen in the measurements, which are not included in the DNS in this study.

Despite the importance of three-dimensional disturbances for the breakdown to

turbulence, the dominance of the two-dimensional fundamental perturbation even far downstream of reattachment is remarkable. Characteristics of the separation bubble have proven to be the same in a DNS with and without forced steady three-dimensional disturbances (Fig. 8). The same holds for the experiment with and without spacers (Fig. 7), suggesting that a large initial disturbance level of three-dimensional disturbances plays only a minor role in the transition process. Instead, the dominating mechanism at work seems to be an absolute secondary instability of three-dimensional disturbances identified by Maucher et al. [16] which is independent of the level of incoming 3-D disturbances. So, differences in amplitude and amplification of DNS and experiment for mode $(0,2)$ are not critical.

Results from stereoscopic PIV measurements

Application of SPIV in a water tunnel is associated with optical problems. Due to large viewing angles, water filled prisms or tanks with mirrors have to be used to align the optical axes of the cameras perpendicular to the boundary of two optically different media. This avoids diffraction effects (astigmatism) and thus makes measurements possible.

Despite a complicated set-up, application of SPIV is superior to a mono-system

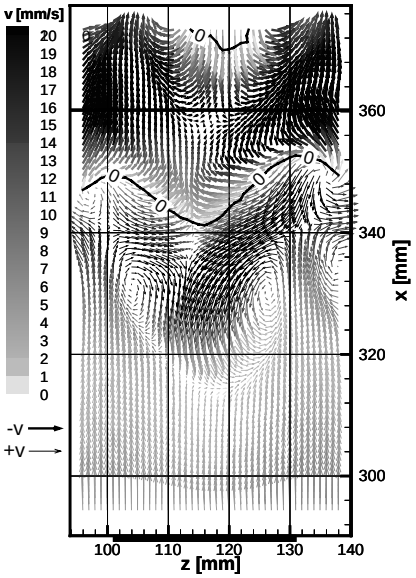

Figure 12 Average of 25 stereo-PIV measurements in the transition region (xz-plane, $y = 16\ mm$). Bar: measurement pos. in Fig.14

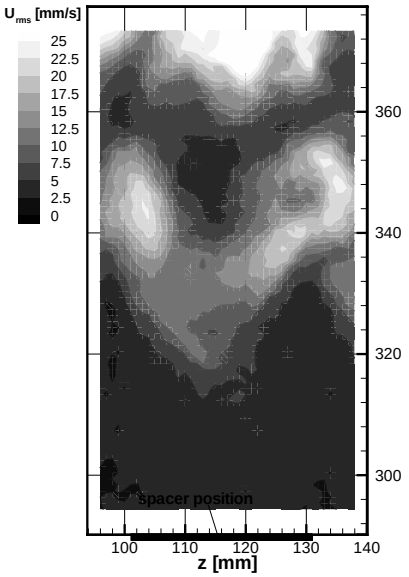

Figure 13 rms-values for the velocity component u obtained by averaging 25 measurements (average shown in Fig.12)

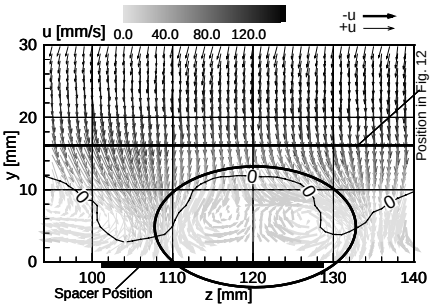

Figure 14 Average of 25 stereo-PIV measurements in the yz-plane at $x = 360\,mm$. Bar: measurement pos. in Fig.12

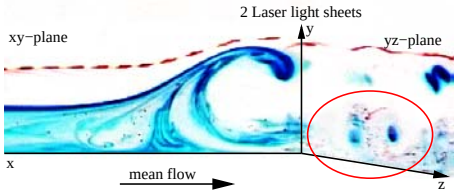

Figure 15 Flow visualization with two simultaneous laser light-sheets in xy-plane and yz-plane

as will be seen in the following results. In the transition region with its strong 3-D development and bidirectional fluctuations, the possibility to capture all three velocity components simultaneously gives an additional insight into 3-D breakdown of the separated shear layer.

Fig. 12 shows the average of 25 phase-locked SPIV measurements with the light sheet aligned parallel to the flat plate ($y = 16\,mm$). Contour colors denote the out-of-plane velocity component v (perpendicular to the light-sheet plane). Rapid 3-D breakdown of the separated shear layer downstream the onset of saturation ($x = 310\,mm$) under the occurrence of counter-rotating vortex pairs is as clearly visible as the dominance of the TS-wave, responsible for strong vortex shedding in the transition region (Fig. 3 and Fig. 15, xy-plane). In the vicinity of these counter-rotating vortices, fluid is shed from inside the LSB up into the separated shear-layer leading to 3-D breakdown. Due to strong velocity gradients in this region, first non-periodicities occur in the flow field, which means high rms-values when multiple measurements are averaged, as can be seen in Fig. 13 for the velocity component u.

Fig. 14 shows the average of 25 SPIV measurements in the yz-plane (light-sheet perpendicular to the mean flow direction) at a streamwise position $x = 360\,mm$ (bar in Fig. 12). The measurements were taken phase-locked at equal phase angle as shown in Fig. 12. Again the out-of-plane component (perpendicular to the light-sheet plane) is denoted by colors (now u). In the vicinity of counter-rotating vortex pairs, a strong reverse flow can be detected.

In Fig. 15 such a vortex pair can be seen from flow visualizations (ellipse). Fluid within the LSB (isolated by the dividing streamline, instantaneous view) is orange colored and one layer is additionally marked with a carpet of hydrogen bubbles. Here, two laser light-sheets were aligned in streamwise direction (yx-plane) and perpendicular to the mean flow (yz-plane), respectively. In the xy-plane the roll-up of the separated shear layer can be seen, while the yz-plane shows the spanwise deformation with 3-D vortex structures in the transition region.

4 Conclusions

A detailed investigation of transition in a laminar separation bubble is given. Thereby, two non-intrusive measurement techniques (LDA, (S)PIV), DNS, and linear stability theory were applied.

A detailed comparison between measurements and numerical calculations of the velocity field in a transitional separation bubble showed very good agreement for time-averaged and 2-D Fourier-analyzed quantities. Transition in a separation bubble in this case is driven by convective primary amplification of 2-D TS waves, mainly determining the size and position of the bubble. Initial level of steady 3-D disturbances in the inflow plays a minor role in the considered transition process. This could be clearly identified from the existing numerical and experimental data.

Due to a new method to measure periodical unsteady phenomena by mono-PIV, measurement time for verification measurements to insure the quality of the experimental set-up could be significantly decreased. Additional stereoscopic PIV measurements gave new and closer insight into the 3-D development of the transitional shear layer with its strong bidirectional fluctuations.

Characteristics of the turbulent boundary layer after reattachment appear to be strongly influenced by the Tollmien-Schlichting mode and remains open to further investigations.

Acknowledgements: The financial support of this research by the Deutsche Forschungsgemeinschaft DFG under grant Wa 424/19-1 was gratefully acknowledged.

References

[1] Watmuff, J., Evolution of a Wave Packet into Vortex Loops in a Laminar Separation Bubble. *J. Fluid Mech.*, 397, 119–169 (1999).

[2] Gaster, M., The Structure and Behaviour of Laminar Separation Bubbles. *AGARD CP 4*, pp. 813–854 (1966).

[3] Fitzgerald, E. J. and Müller, T. J., Measurements in a Separation Bubble on an Airfoil Using Laser Velocimetry. *AIAA Journal*, **28(4)** (1988).

[4] Strunz, M. and Speth, J. F., A New Laminar Water Tunnel to Study the Transition Process in a Blasius Boundary Layer and in a Separation Bubble and a New Tool for Industrial Aerodynamics and Hydrodynamic Research. *AGARD CP-413*, pp. 25–1–25–5 (1987).

[5] Wiegand, T., *Experimentelle Untersuchungen zum laminar-turbulenten Transitionsprozess eines Wellenzuges in einer Plattengrenzschicht*. Dissertation, Universität Stuttgart (1996).

[6] Boiko, A. V., Grek, G. R., Dovgal, A. V. and Koslov, V. V., *The Origin of Turbulance in Near-Wall Flows*. Springer Verlag (2002).

[7] Alam, M. and Sandham, N., Direct numerical simulation of 'short' laminar separation bubbles with turbulent reattachment. *J. Fluid Mech.*, 410, 1–28 (2000).

[8] Rist, U., *Zur Instabilität und Transition in laminaren Ablöseblasen*. Habilitation, Universität Stuttgart, Shaker Verlag, Aachen (1998).

[9] Kruse, M. and Wagner, S., LDA Measurements of Laminar-Turbulent Transition in a Flat-Plate Boundary Layer. 8^{th} International Symposium on Applications of Laser Techniques to Fluid Mechanics, 8.–11. July, Lisbon, Portugal (1996).

[10] Kruse, M., *Einsatz der Laser-Doppler-Anemometrie zur Untersuchung des laminar-turbulenten Grenzschichtumschlags an der ebenen Platte*. Dissertation, Universität Stuttgart (1997).

[11] Maucher, U., Rist, U. and Wagner, S., Refined Interaction Method for Direct Numerical Simulation of Transition in Separation Bubbles. *AIAA Journal.*, **38(8)**, 1385–1393 (2000).

[12] Marxen, O., Lang, M., Rist, U. and Wagner, S., A Combined Experimental/Numerical Study of Unsteady Phenomena in a Laminar Separation Bubble. In: *Proceedings of IUTAM Symposium "Unsteady Separated Flows" (CD-Rom)*. Toulouse (2002).

[13] Lang, M., Marxen, O., Rist, U., Wagner, S. and Würz, W., LDA-Messungen zur Transition in einer laminaren Ablöseblase. In: *Lasermethoden in der Strömungsmesstechnik*. 8. Fachtagung der GALA, 12.–14. Sep. 2000, Freising-Weihenstephan, Shaker Verlag, Aachen (2000).

[14] Ronneberger, O., Raffel, M. and Kompenhans, J., Advanced Evaluation Algorithms for Standard and Dual Plane Particle Image Velocimetry. 9th International Symposium on Applications of Laser Techniques to Fluid Mechanics, Lisbon, Portugal (1998).

[15] Lang, M., Marxen, O., Rist, U. and Wagner, S., Experimental and Numerical Investigations on Transition in a Laminar Separation Bubble. In: Wagner, Rist, Heinemann and Hilbig (eds.), *Notes on Numerical Fluid Mechanics, New Results in Numerical and Experimental Fluid Mechanics*, pp. 207–214. 12^{th} Stab Symposium 2000, Stuttgart, Springer Verlag, Heidelberg (2000).

[16] Maucher, U., Rist, U. and Wagner, S., Transitional Structures in a Laminar Separation Bubble. In: W. Nitsche, H. Heinemann and R. Hilbig (eds.), *Notes on Numerical Fluid Mechanics*, vol. 72, pp. 307–314. Vieweg Verlag, Wiesbaden (1999), 11^{th} Stab Symposium 98, Berlin.

[17] Augustin, K., Rist, U. and Wagner, S., Numerical Simulation of Laminar Separation-Bubble Control. In: Wagner, Rist, Heinemann and Hilbig (eds.), *Notes on Numerical Fluid Mechanics, New Results in Numerical and Experimental Fluid Mechanics*, pp. 181–188. 12^{th} Stab Symposium 2000, Stuttgart, Springer Verlag, Heidelberg (2000).

[18] Lang, M., Rist, U. and Wagner, S., Investigations on Disturbance Amplification in a Laminar Separation Bubble by Means of LDA and PIV. 11^{th} International Symposium on Applications of Laser Techniques to Fluid Mechanics, 8.–11. July, Lisbon, Portugal (2002).

[19] Marxen, O., Rist, U. and Wagner, S., The Effect of Spanwise-Modulated Disturbances on Transition in a 2-D Separated Boundary Layer. AIAA–Paper 2003-0789 (2003).